Estimating Bathymetry of Cross River in Nigeria using Remote Sensing Technique

Akwaowo U. Ekpa[1], Oliver C. Ojinnaka[2]
[1]Department of Geoinformatics and Surveying University of Uyo, Akwa Ibom State, Nigeria.
[2]Department of Geoinformatics and Surveying University of Nigeria, Nsukka, Enugu State, Nigeria

Abstract

The orthodox sonar systems employed in charting the extensive and shallow coastal waters of Nigeria have been constrained by policies, cost implications, environmental hostilities, and failure to access shallow waters due to possible grounding, etc. Consequently, a large portion of Nigerian coastal waters has remained uncharted or un-updated. This paper discusses the application of satellite remote sensing method in near-shore bathymetry of a section of Cross River in Nigeria. The data employed are multispectral Landsat-7 ETM+, sounded depths, admiralty chart data and tidal data. Atmospheric correction of the satellite image was performed using Improved Image-Based Dark Object Subtraction (DOS) Model, while the Ratio Model was employed to estimate the bathymetric depths. The predicted tidal data was used to reduce the sounded depths and Landsat-derived depths to the same Chart datum for ease of evaluation. Validation of the Landsat-7 ETM+ derived depths with reduced sounded and chart depths yielded Coefficient of Determinations, R^2 = 0.821 and 0.716 respectively. The results therefore show that the technique is reliable for rapid bathymetry and monitoring of near-shore coastal shallow waters, and consequently aid in charting the coastal rivers.

Keywords — *Bathymetry, Remote Sensing, Derived Image Depths, Coastal Waters, Landsat-7 ETM+, Cross River, Chart Depths.*

I. INTRODUCTION

Many coastal environment of the world have not been fully surveyed, and many that have been surveyed are seriously outdated [4]. This scenario is a typical in Nigeria, where there is yet to be a comprehensive navigational charts for her in-land and coastal water ways. And these could be attributed to the challenges associated with the orthodox sonar techniques of acquiring bathymetric data.

For a nation to make maximum utilization of her marine resources the water ways must be charted and regularly updated. Unfortunately, due to the different disciplines involved, highly specialized techniques and skills required, high cost of marine operations and the apparent lack of awareness of the importance of these charts, it has been difficult for most developing nations of the world to pay serious attention to the charting of their water ways. In Nigeria, for instance, charting is undertaken by the Nigerian Ports Plc, the Nigerian Inland Waterways Authority (NIWA), the Nigerian Navy and some other Private Organizations, with each concentrating within the limits of her specific areas of operations [14]. Whereas, this is the reverse in many developed countries like the United States of America where the Meteorology and Oceanography Community (METOC) of the United States Navy is tasked with the role of obtaining, storing and updating a worldwide database of ocean bathymetry, known as Digital Bathymetric Data Base (DBDB). The office of Naval Research uses the DBDB as an input for various modeling algorithms, (acoustic prediction, tide and surf forecasting, weapon system); planning charts (command and control, mission planning, tactical decision aids); and for coastal zone management, environmental monitoring, engineering/construction, and resource development/exploration [4].

The coastal areas also are often characterized by high population density, heavy maritime traffic and vulnerable natural ecosystems like mangrove, creeks, lagoons or coral reefs. And the need for environmental researches, investigation of the seabed morphology, and monitoring of navigational channels for safety, to ensure proper management of resources in the coastal zones through bathymetric survey. Because of this, “Reference [11], affirmed that sea depth changes because of erosion and sedimentation processes, and bathymetry must often be accurately updated”. Also, because bathymetry is also essential for modelling and predicting coastal storm surge and flooding, oceanic circulation and tsunami propagation [7].

In the past, the various methods employed to obtain bathymetric depths ranged from lead weight line, single beam sounder (echo sounder), multi-beam and side scan sonar systems, and the LiDAR (Light Detection and Ranging) system. These methods, though produced very accurate results, have associated difficulties. These include heavy and expensive equipment, high labour input, extensive data processing and slow speed of operation. Duration and extent of coverage is limited by ship’s fuel capacity; and possibility of grounding in shallow areas (of <5m) poses danger in near-shore bathymetry. To this end, the sonar methods have been disproportionately concentrated to areas with high marine traffic, high population density and easy accessibility. Whereas, “denied areas”, remote and isolated, have been left out

in such bathymetric mapping, due to the above limitations. The rigorous field processes of these methods have also limited their ability to be used in mapping the all the nooks and crannies of the marine environment.

Since 1970, satellite remote sensing technology was gradually adopted as an alternative in clear water bathymetry mapping to minimize field work. The synoptic view, easy access, and dynamic nature have made remote sensing approach a rather cost effective way to provide quick solutions to bathymetry mapping for studies of the fast-changing coastal environment [18]. Although optical remote sensing sensors are limited in respect of depth of penetration (DOP) and constrained by water turbidity, they provide a faster and lower-cost alternative to ship-borne sonar bathymetric mapping in shallow water [10]. The remote sensing techniques are especially suitable for remote areas or hazardous coastal areas (e.g., with high surf) where ship operations are logistically problematic. In addition, they also have wide data availability, synoptic surface coverage, minimal field operations, and high spatial resolution. However, it requires adequate carefulness during calibration of the remotely sensed images in order to ensure that the extracted depth information is accurate.

Remote sensing from satellite platforms has been an essential tool to measure and study terrestrial, atmospheric, and oceanic properties. The feasibility of deriving bathymetric estimates from remote sensing imagery was first demonstrated using aerial photographs over clear shallow water [6]. The technique was expanded to include the use of passive optical multi-spectral satellite imagery such as Landsat [6], IKONOS [17], QuickBird [1], Worldview-2 [9]. The applications of optical remote sensing have been effectively used in shallow marine environments to determine water depths, to augment current navigational charts [1]; as a cost-effective complement to traditional in-situ sounding methods [10]; and to produce bathymetric maps [11]. Hence, this paper employs the technique of satellite remote sensing, using multispectral satellite image of Landsat 7 ETM+, to estimate bathymetric depths of Nigerian coastal shallow waters for the purposes of monitoring possible changes of seabed topography.

II. MATERIALS AND METHODS

A. *Study Area*

The study area is the access channel from the Atlantic Ocean on the South to the Calabar Port (Export Processing Zone (EPZ)) northward, in Cross River State, Nigeria. It naturally serves as the coastal boundaries between Akwa Ibom State on the west and Cross River State on the north-east, both in the South-South Region (Niger Delta region) of Nigeria; and Bakassi Peninsula on the east. It lies between longitude 8^{o} 14' E and 8^{o} 32' E, and latitude 4^{o} 31' N to 4^{o} 49' N (see Fig. 1). Downwardly, the cross-sectional distance of the river is about 16 kilometers. Since the river empties into the Bight of Bonny, it has the potential of being influenced by hydrological dynamics from the Atlantic Ocean. Being the strategic entrance route from the Atlantic Ocean to Calabar Port, Export Processing Zone (EPZ), it is shown on the Admiralty Chart (Sheet No. 3433) titled, "Approaches to Calabar". The physical relief of the coastal lands of Akwa Ibom State is characterized by deltas, estuaries, lagoons, creeks and swamps. The swamps are tidal mudflats in nature. The vegetation on the coastal lands are generally made up of flood plain mangrove, brackish or saline mangroves and salt-water swamp forests. The economic significance of the river and its environs comprise of abundant oil and gas reserves, fishing, marine transportation, etc.

The mean annual rainfall in the area is about 4050mm, and the rainy season lasts from May to October, while the duration of the dry season is November to April.

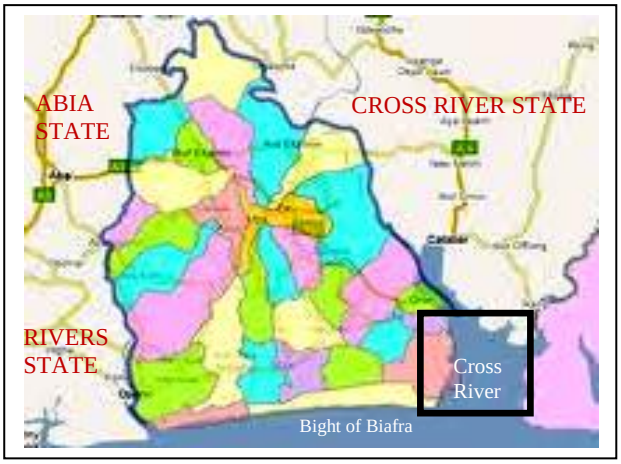

Fig. 1: Akwa Ibom State Map with insert of Cross River and part of Bight of Bonny
(Source: http://www.google.com.ng/search.images)

B. *Methodology*

The methodological approach adopted for this study was as described in the flow chart in Fig. 2. The approach was categorized into three phases; data acquisition, data preparation, and results and analyses. Hence, the discussions on the steps systematically followed this order.

1. *Field Equipment*

The equipment used for bathymetric data were:

- SDE-28 Echo Sounder (Model No. D10280806) with other accessories to obtain sounded depths on the river.
- Ashtech ProMark™ 3 Differential Global Position System (DGPS) - used to coordinate the Bench Marks (BMs) and fixing positions of sounded points.
- Staff Gauge: A 4m tide gauge to obtain hourly daily tidal heights of the river.

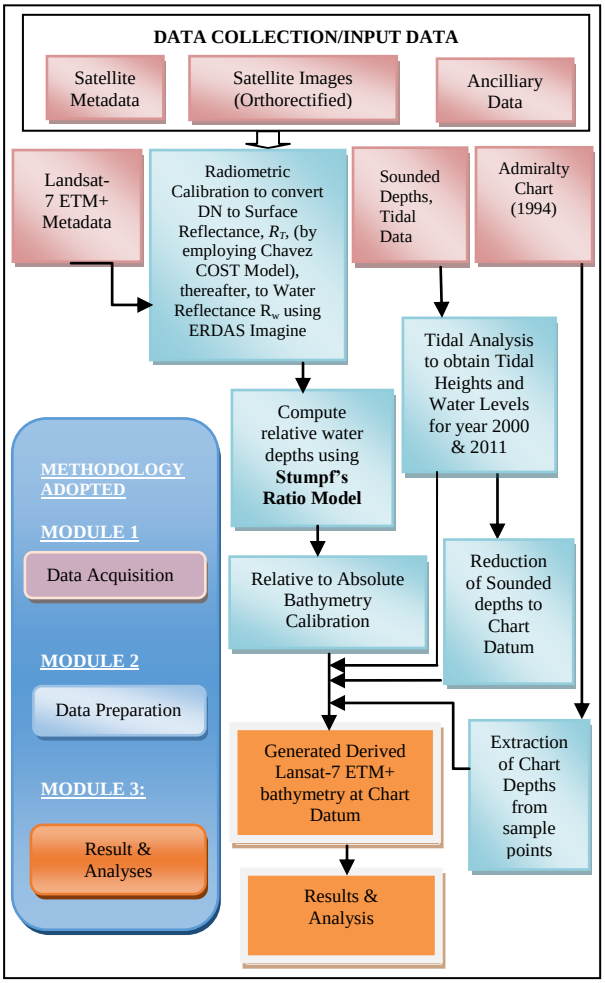

Fig. 2: Flow Chart of the Methodology

2. *Datasets Acquisition*

2.1. *Spectral Datasets*

The image dataset used for this study was Landsat 7 ETM+ image set acquired on December 10, 2000 and downloaded from the Global Land Cover Facility (GLCF) archive images data ***(http:glcfapp.umias.umd.edu***). It was processed through Level 1 Product Generation System (LPGS) of the United States Geological Surveys (USGS). The path/row of the image was 187/057. The acquired image was level 1G and had been ortho-rectified and radiometrically calibrated by USGS (see Figure 3).

2.2 *Metadata Sets*

The calibration parameters from the header file of the Landsat-7 ETM+ included date of acquisition, sun elevation angle, path/row of image number, gain, bias (offset), maximum and minimum radiance values, sun azimuth, cloud cover, image projection, reference datum and ellipsoid.

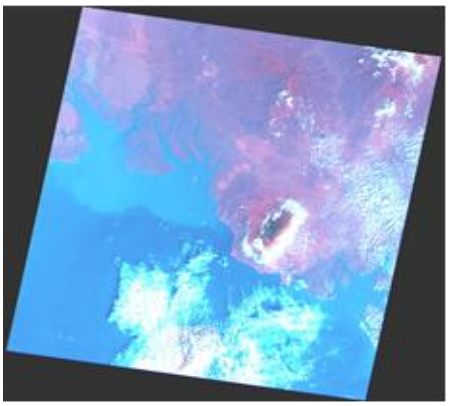

Fig. 3: Downloaded Stacked Image for Band 1 – 5 & 7 (Source: http:glcfapp.umias.umd.edu)

2.2.1 *Input Parameters*

The parameters of Landsat-7 ETM+ obtained from the image header file attached to the image by the provider (Earth Resources Observation and Science (EROS) Center) are shown in table I below.

Table I: Parameters of Landsat-7 ETM+ 2000.

SENSOR	L7 ETM+ (GROUP - L1G)
Date of Acquisition	December 10, 2000
Julian Day	345
Acquisition Time	09 : 29 :11 (GMT)
Bands	1 – 7 (Reflective) and Pan exclude 6 (thermal)
Path/Row	187/057
Pixel Size	30m
Factor Scale	4 default
Solar Zenith Angle	θ = (90 – 52.0942488)
Sun Azimuth	137.2207378
Calibrated File	L7CPF20001001_20001231_07
Model of solar Region	Others. TYPE: Tropical Ocean
Cloud Cover	10
Visibility	30 km
Reference Datum	WGS 84
Zone Number	32
Map Projection	UTM
Resolutions	Bands 1 – 7 (30m), Band 6 (60m), and Pan (15m)

(Sources: Image Header File and – http://landsat.usg.gov//L7_Pend_Acq/y/2000/Dec/Dec/-10-2000.txt

2.3 *Tidal Datasets*

A manual staff gauge was established to obtain tidal information. The staff gauge was a 4m graduated (at 1cm interval), mounted on the seabed. The location of the tide gauge station was at the Nigerian Navy Forward Operating Base, Ibaka in Mbo L.G.A, Akwa Ibom State, Nigeria (see Figure 4). Tidal heights reading on hourly basis were obtained for a period of 36 days. The tidal values were used to reduce the

sounded depths to chart datum, and also to carry out tidal analysis. The obtained tidal constants for 28 constituents were used to predict tide and water level for time and date image was acquired. The heights of the BMs were obtained on WGS 84 datum using Ashtech ProMark™ 3 DGPS (see Figure 5: DGPS on the control BM 20).

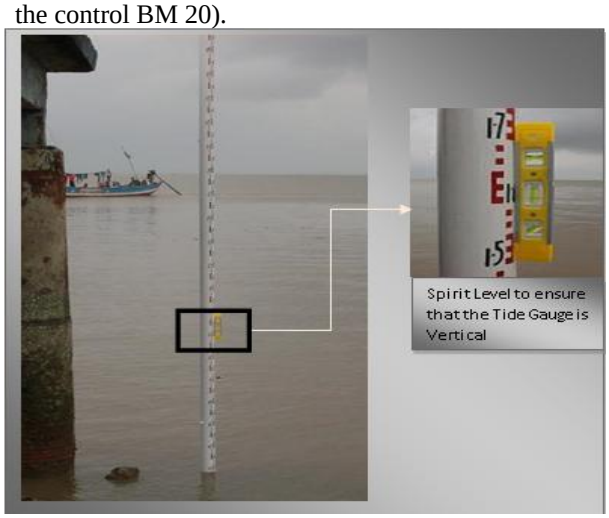

Fig. 4: Established Tide Pole Gauge

Fig. 5: Ashtech ProMark™ on the BM Control

2.4 *Bathymetric Datasets*

Field survey to acquire bathymetric depths of cross sections and selected points on the river was carried out using SDE 28 Echo Sounder, with Ashtech ProMark™ 3 DGPS to fix the positions of the sounded depths. The sounded depths were reduced to chart datum using the predicted tidal heights. Also, depths information referenced to chart datum were also extracted from an Admiralty Chart of Approaches to Calabar (Sheet No. 3433 scale 1: 50,000) published in 1994.

3. *Data Preparation*

The algorithm used in the preparation of the spectral and bathymetric data for water depth estimation were as shown in Figure 6.

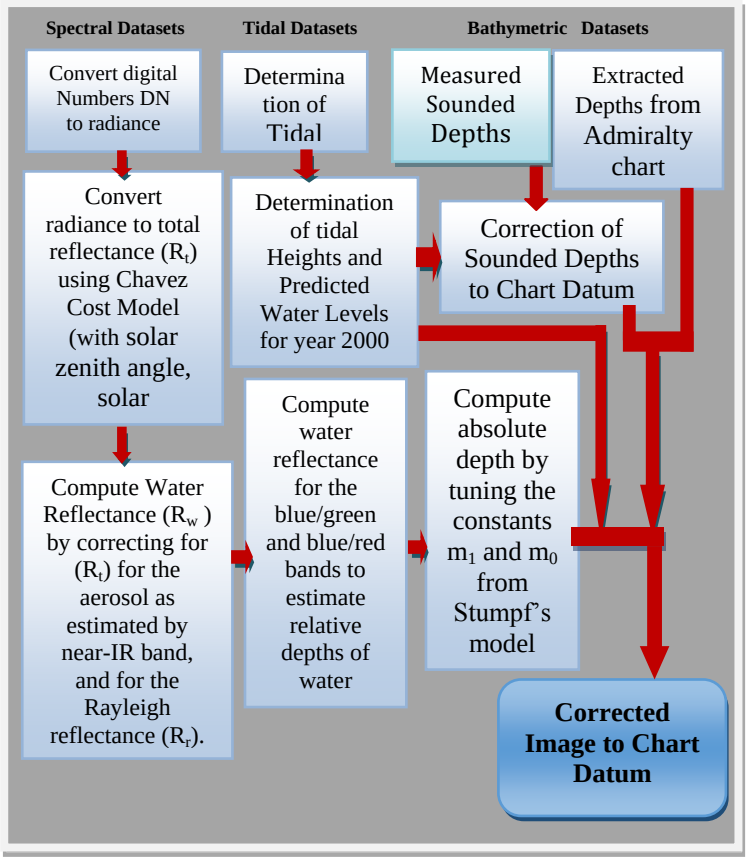

Fig. 6: Algorithm for Data Preparation

3.1 *Geometric Image Correction*

Geometric correction aimed at rectifying the image coordinates to existing ground coordinates in a specified projection system and datum. Landsat-7 ETM+ image being a level 1G fully processed product implied that the image was geometrically standardized. Hence, geometric correction was not performed on the image which already had been processed by the image provider.

3.2 *Atmospheric Correction*

The objective of atmospheric correction was to convert remotely sensed DN to ground surface reflectance. The processes employed are listed below.

- Conversion of DN to Surface Reflectance
- Determination of Water Reflectance

3.2.1 *Conversion of DN to Surface Reflectance*

The Improved Image-Based DOS Model was used to convert DN to surface or total reflectance using Chavez COST method as shown in the equation *(3.1)* below. This model is a Web-Based tool *(http://earth.gis.usu.edu/imagestd/)* to create the Image-based calibration spatial model (in .gmd file). The option of entering extracted parameters directly into the tool, that is, 'without header file name' being linked online to the image header file was adopted. The output model (.gmd file), the output metadata files (.txt file), and the graphic model were created. Thus, atmospherically corrected (reflectance) image

from the COST model was obtained as shown in Figure 7.

$$R_T(\lambda) = \frac{\pi\left((DN_\lambda \times Gain_\lambda + Bias_\lambda) - (H_\lambda \times Gain_\lambda + Bias_\lambda)\right) \times D^2}{E_{SUN\lambda} \times \left[COS\left((90-\theta) \times \frac{\pi}{180}\right)\right] \times \tau} \quad (3.1)$$

Where,

R_T = is the total reflectance for spectral band λ

DN_λ = Digital Number for Spectral Band λ

$Gain_\lambda$ = Radiometric Gain

$Bias_\lambda$= Radiometric Bias (Offset)

π = Mathematical Constant 3.1415926

Cos (90 - θ) = Sun Zenith Angle. (θ is the solar elevation)

D^2 = Square of Normalized Earth-Sun Distance = [1 – 0.01674 x Cos (0.9856 x (JD-4))]^2, [13].

To convert the units to radians is simply to multiply by π/180.

$E_{Band}\lambda$ = Exo-atmospheric Solar Irradiance for Spectral Band λ (Same as $E_{SUN}\lambda$).

H_λ = Digital Number representing Dark Object for Spectral Band λ

τ = Atmospheric Transmittance expressed as: = (Cos ((90 – θ) x π/180)) for COST model, [3].

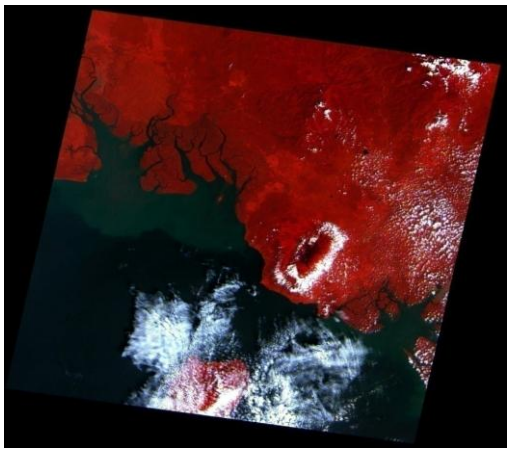

Fig. 7: Surface Reflectance Image using Improved Image-Based Model

3.2.2 *Determination of Water Reflectance*

The model to determine water reflectance, R_w, of a spectral band is as defined in equation *(3.2).*

$$R_w = \frac{\pi L_w(\lambda)}{E_d(\lambda)} \quad (3.2)$$

Where,

L_w = the water-leaving radiance

E_d = the downwelling irradiance entering the water

λ = the wavelength of the spectral band.

The water-leaving radiance, L_w, and the downwelling irradiance, E_d, parameters are physical quantities which are obtained using a spectroradiometer. Howbeit, due to certain difficulties in obtaining these physical quantities, an alternative approach was adopted. "Reference [17] and [18] showed that Water Reflectance, $R_w(\lambda)$, could be determined using the model":

$$R_w(\lambda_i) = R_T(\lambda_i) - Y(\lambda_i)R_T(\lambda_{IR}) - R_r(\lambda_i) \quad (3.3)$$

Where;

R_T = is the total reflectance for spectral band λ.

Y = the constant to correct for spectral variation (equivalent to the Angstrom exponent in Gordon et al. [5], [17].

$R_r(\lambda)$ = Rayleigh Reflectance is estimated by the deep water reflectance of the wavelength (λ) Subscript ***i*** and IR = denote the wavelengths of the visible and near-IR spectral bands.

The reflectance of water (R_w) was be found by correcting the total reflectance, R_T for the aerosol and surface reflectance, as estimated by the near-IR band, and for the Rayleigh reflectance, R_r [17]. This step was used to obtain water reflectance images for the three Bands (blue, green and red) as shown in Figures 8(a), (b) and (c) respectively. "Reference [18] also validated this approach, that the correction presumed a maritime atmosphere with a spectral variation similar to that of the water surface reflectance, and the assumption was reasonable for the Landsat-7 ETM+".

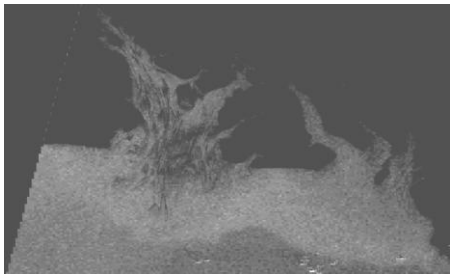

Fig. 8(a): Water Reflectance Image of Blue Band

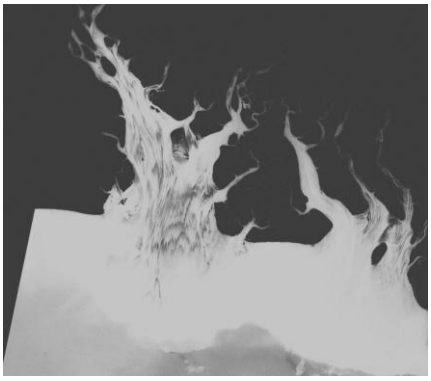

Fig. 8(b): Water Reflectance Image of Green Band

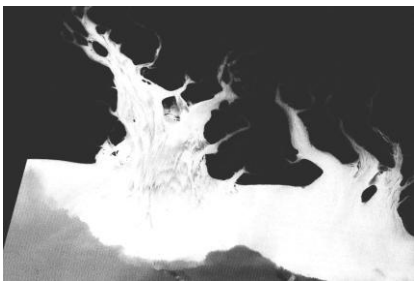

Fig. 8(c): Water Reflectance Image of Red Band

4. Processing of Tidal Data and Sounded Data Reduction

Due to unavailable pedicted tidal information for the river, tabulated harmonic tidal constants for 29 constituents which included **M_2, S_2, K_1 and O_1** were extracted from the Admiralty Manuals for Hydrographic Surveyors for this location. These constants were processed using University of Nigeria Tidal Analysis and Prediction Program (UNITAPP) to predict reduced water levels at chart datum for the years 2000 (year of image acquisition) and 2011 (year of sounding operation) respectively. The predicted tidal value was then used to reduce to the sounded depths to chart datum.

5. Extraction of Water Depths

The two basic methods for deriving bathymetric data from remote sensing imagery are the Linear and Ratio Methods. The Linear methods (linear inversion methods) are based on several implicit assumptions and range in complexity. They calculate bottom reflectance assuming that water properties are homogeneous and light is attenuated exponentially with depth [6]. The Ratio Method (non- linear inversion method) developed by [17] was based on the ratio of two or more wavelengths. "Reference [17] expanded on the linear model original of water depth derivation and offered more accurate depths estimation over variable bottom types (reflectance) in deep and shallow environment by using ratio of reflectance".

This study adopted the Ratio Model to estimate water depths from the image by using the blue/green and blue/red ratios of image wavelengths. The model states that:

$$z(depth) = m_1 \frac{ln[nR_w(\lambda_i)]}{ln[nR_w(\lambda_j)]} - m_0 \qquad (3.4)$$

Where,

m_1 = a tunable constant to scale the ratio to depth.
n = a constant for all areas to ensure that the algorithm is positive under all circumstances.
m_0 = offset for a depth of 0m
$R_w(\lambda_i \text{ or } _j)$ = Water Reflectance of a particular wave band.

The first steps to determine bathymetry from the image was to determine relative bathymetry using natural log transform of the reflectance values below.

$$\frac{ln[1000*R_w(\lambda_i)]}{ln[1000*R_w(\lambda_j)]} \qquad (3.5)$$

Where, the water reflectance values were multiplied by 1000 (the value of n) to ensure that the logarithms remain positive for all reflectance values. This was followed by scaling the relative bathymetry to absolute bathymetry. Thus, series of points from the Admiralty Nautical chart were extracted as in-situ data, and regressed against the relative bathymetry values to obtain absolute bathymetry for the entire image. Thereafter, the predicted water level value on the date of image acquisition was used to reduce the Landsat-7 ETM+ derived water depths to chart datum.

III. RESULTS AND DISCUSSIONS

A. Results and Analyses

The bathymetry for Cross River was generated from the multispectral Landsat 7 ETM+ imagery. The depths range of the river was between 0m – 14m. The characteristics of the seabed were not classified in this study, bearing in mind the fact that the ratio model could be used over variable bottom [17]. The derived bathymetry from the combination of blue/red wavelengths ratio, depicted the seabed topography of the entire area better when compared to the blue/green ratio. This was because the blue/red ratio produces higher depths accuracy in shallow water regions (< 5m) than the blue/green ratio. Figure 9 was generated from blue/red combination covering the study area, and it depicted the changes in depths towards the ocean. While Figure 10 shows details of the seabed topography generated from blue/green ratio for the study area.

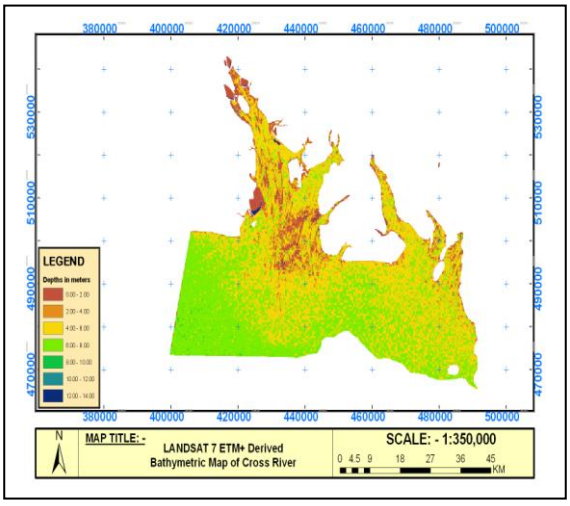

Fig. 9: Landsat-7 ETM+ Derived Depths of Cross River using Blue/Red Ratio

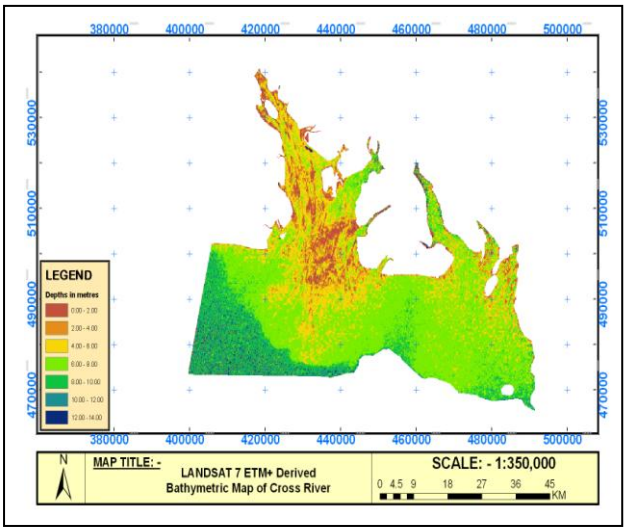

Fig. 10: Landsat-7 ETM+ Derived Depths of Cross River using Blue/Green Ratio

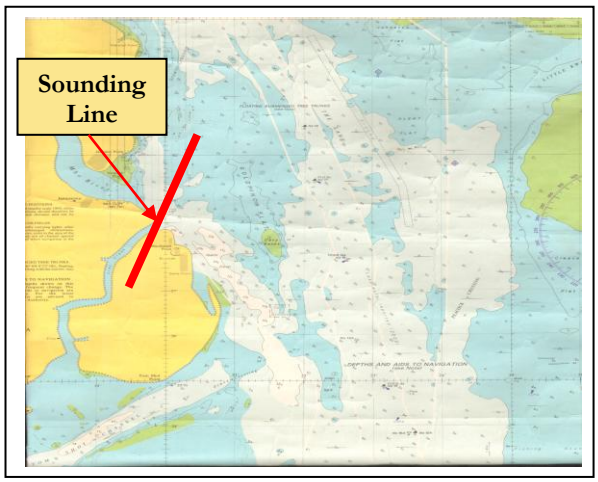

Fig. 12: A portion of the Admiralty Chart of Calabar Channels (published in 1994)

1. *Analyses of Results*

Analyses of the results of the estimated image depths were done in two phases. The first phase involved comparing the estimated image depths with the reduced sounded and chart depths. Secondly, the differences (errors) obtained from the comparisons were statistically analyzed to ascertain the correlation and the relative accuracy of the estimated image depths from the sounded and chart depths.

i) Comparison of Bathymetric Depths

A comparison of the Landsat-7 ETM+ derived image with the Admiralty Chart revealed good similarities in depths and patterns of the seabed (Figures 11 and 12), though, slight differences were observed in certain areas. Another important characteristic of the river was the extent of shallow depths, which was a typical characteristics of coastal waters in the Africa region.

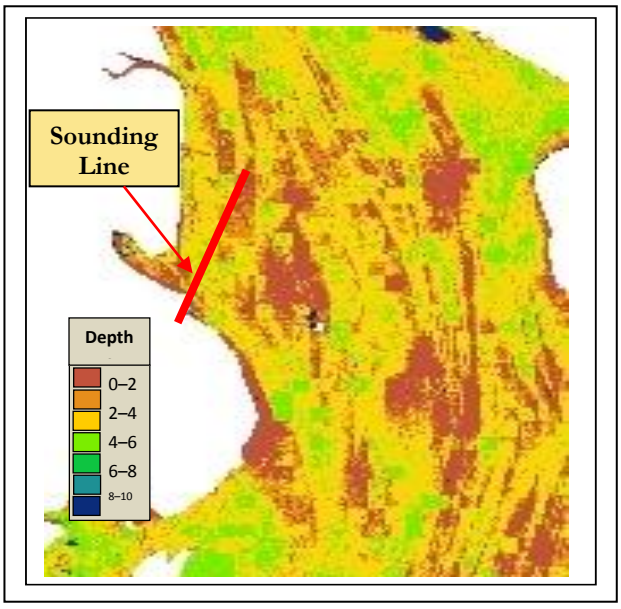

Fig. 11: A portion of Landsat 7 ETM+ (2000) Derived Image Depths

Also, two sets of validations were carried out on the estimated image depths – firstly, comparing the estimated image depths with sounded depths and chart depths simultaneously (for the area where sounded depths were obtained); while the second set required comparing randomly selection of estimated image depths with their corresponding chart depths. In the first comparison, the estimated image depths obtained from the blue/red ratio was used, because the extent of the area investigated by sounding was shallow (0 and 5m). Whereas, in the second aspect, the estimated depths results obtained from both blue/green and blue/red ratios were used separately with the chart depths. In the first instance, the measured sounding points covered a distance of about 4.2km. Depths values of

Table II: Comparison of Image, Sounded and Chart Depths reduced to Chart Datum

DIST (m)	FIXES	SOUNDED DEPTHS (m)	CHART DEPTHS (m)	IMAGE DEPTHS (BLUE/RED) m)	NORTHINGS (m)	EASTINGS (m)
00.00	LIN A	5.03	5.10	5.20	514172.943	424545.935
50.00	LIN B	5.00	5.40	5.50	514216.020	424571.609
110.70	LIN C	4.17	4.20	4.50	514266.620	424604.934
182.20	LIN D	3.47	3.00	3.50	514329.166	424639.722
233.30	LIN F	2.69	2.80	3.10	514375.038	424662.495
307.10	LIN G	1.42	2.20	2.30	514447.868	424682.809
360.90	LIN H	0.90	1.10	2.10	514500.303	424697.866
433.90	LIN I	0.73	0.80	1.60	514572.464	424715.079
485.12	LIN J	0.95	0.90	1.50	514623.884	424724.806
525.72	LIN K	1.03	0.90	1.50	514663.555	424734.819
607.70	LIN L	1.05	0.90	1.20	514744.660	424751.903
712.00	LIN N	0.75	0.80	0.80	514846.750	424775.930
780.70	LIN O	0.66	0.70	0.80	514908.971	424806.200
819.90	LIN P	0.50	0.50	0.60	514946.017	424818.919
858.50	LIN Q	0.44	0.50	0.90	514982.794	424830.758
896.70	LIN R	0.38	0.40	0.60	515020.512	424838.655
934.70	LIN S	0.32	0.40	0.50	515056.954	424849.537
972.70	LIN T	0.35	0.30	0.50	515092.651	424862.511
1010.80	LIN U	0.32	0.30	0.50	515128.391	424875.698
1049.30	LIN V	0.30	0.30	0.50	515165.230	424887.250
1088.00	LIN W	0.30	0.30	0.50	515202.504	424897.938
1127.16	LIN X	0.22	0.20	0.40	515240.227	424908.423
1165.90	LIN Y	0.26	0.30	0.40	515277.113	424920.204
1204.40	LIN Z	0.27	0.20	0.30	515313.030	424934.252
1242.90	LIO 0	0.30	0.20	0.50	515348.667	424949.243
1281.40	LIO 1	0.23	0.20	0.40	515383.944	424964.809
1320.10	LIO 2	0.25	0.30	0.30	515419.978	424979.080
1359.30	LIO 3	0.23	0.30	0.30	515456.808	424992.573
1398.80	LIO 4	0.28	0.30	0.30	515494.195	425005.125
1439.20	LIO 5	0.73	0.60	0.90	515530.555	425023.692
1477.60	LIO 6	0.40	0.60	1.10	515564.701	425042.241
1516.00	LIO 7	0.49	0.70	0.80	515596.998	425065.930
1556.40	LIO 8	0.59	0.60	0.60	515634.591	425080.769
1597.50	LIO 9	0.79	0.80	0.80	515675.589	425088.312
1638.60	LIOA	0.84	0.90	1.10	515714.131	425102.413
1679.30	LIO B	0.90	1.40	1.20	515752.544	425116.054
1720.50	LIO C	1.00	2.20	1.20	515792.315	425127.124
1761.16	LIO D	1.09	2.30	1.40	515829.099	425144.956
1802.37	LIO E	1.33	2.50	1.50	515866.728	425162.079
1844.33	LIO F	1.97	2.60	2.30	515905.819	425177.358
1886.08	LIO G	2.45	3.20	3.00	515943.439	425196.056

the same sounding positions were extracted from their corresponding image and the Admiralty Chart depths positions respectively (Table II). The three sets of depths values were concurrently plotted to show the seabed trend and possible variations in heights differences (Figure 13).

DIST (m)	FIXES	SOUNDED DEPTHS (m)	CHART DEPTHS (m)	IMAGE DEPTHS (m) (BLUE/RED)	NORTHINGS (m)	EASTINGS (m)
1927.07	LIO H	2.64	3.60	3.00	515979.685	425216.227
1967.21	LIO I	3.48	3.70	3.30	516013.776	425239.657
2006.86	LIO K	4.01	4.20	3.90	516046.173	425265.989
2089.01	LIO L	4.75	4.80	4.60	516115.532	425314.261
2130.75	LIO M	5.43	4.70	5.40	516151.967	425335.592
2166.40	LIO N	5.56	4.20	5.30	516183.143	425353.629
2197.38	LIO O	5.58	4.30	5.50	516209.800	425370.389
2235.90	LIO P	5.67	4.40	5.30	516241.807	425393.902
2311.64	LIO Q	5.53	4.40	5.70	516303.373	425443.131
2401.11	LIO R	5.42	4.80	5.20	516377.759	425496.773
2448.93	LIO S	5.86	5.40	5.50	516421.896	425515.194
2496.29	LIO T	5.34	5.10	5.70	516464.201	425536.983
2544.04	LIO U	5.24	5.20	5.00	516501.669	425565.430
2577.90	LIO V	5.11	5.40	5.20	516530.570	425588.618
2619.02	LIO W	5.02	5.40	5.20	516565.118	425612.136
2664.15	LIO X	4.93	5.50	4.90	516600.601	425643.274
2710.87	LIO Y	4.88	5.70	4.40	516640.350	425668.755
2757.91	LIO Z	4.69	5.80	5.00	516681.732	425691.373
2803.80	LIP 0	4.68	6.00	5.00	516721.564	425714.621
2849.46	LIP 1	4.66	6.60	6.20	516762.236	425735.672
2894.55	LIP 2	4.59	6.50	6.20	516802.150	425756.595
2964.17	LIP 3	4.60	6.40	6.40	516864.143	425788.408
3034.54	LIP 4	4.46	6.30	6.20	516923.444	425827.802
3091.95	LIP 5	4.39	6.30	6.20	516966.542	425871.071
3141.84	LIP 6	4.41	6.20	6.20	517003.304	425909.826
3196.74	LIP 7	4.36	6.30	6.20	517048.176	425943.138
3245.37	LIP 8	4.22	6.20	6.30	517090.098	425968.123
3293.81	LIP 9	4.11	6.00	6.10	517130.679	425995.420
3341.50	LIP A	4.12	5.00	5.10	517170.170	426023.174
3390.88	LIP B	3.93	5.40	6.10	517216.825	426040.213
3440.99	LIP C	3.78	5.00	5.50	517260.630	426062.666
2488.12	LIP D	3.74	4.80	4.90	517301.111	426089.132
3534.98	LIP E	3.62	4.80	4.90	517337.895	426120.475
3581.77	LIP F	3.57	4.80	5.40	517374.769	426151.355
3628.27	LIP G	3.57	4.40	4.80	517412.609	426179.611
3675.63	LIP H	3.39	4.50	5.30	517453.743	426203.222
3722.57	LIP I	3.25	4.40	4.80	517497.407	426220.883
3769.62	LIP J	3.10	4.20	4.30	517541.642	426237.656
3833.51	LIP K	3.02	4.20	5.70	517596.855	426270.059
3859.20	LIP L	2.86	4.20	7.10	517609.378	426302.160
3906.63	LIP M	2.73	4.20	7.10	517651.934	426323.106
3998.06	LIP O	2.65	4.00	6.50	517727.533	426376.063
4080.88	LIP P	2.48	3.00	3.60	517786.216	426442.730
4139.78	LIP R	2.71	3.40	3.70	517839.910	426467.155

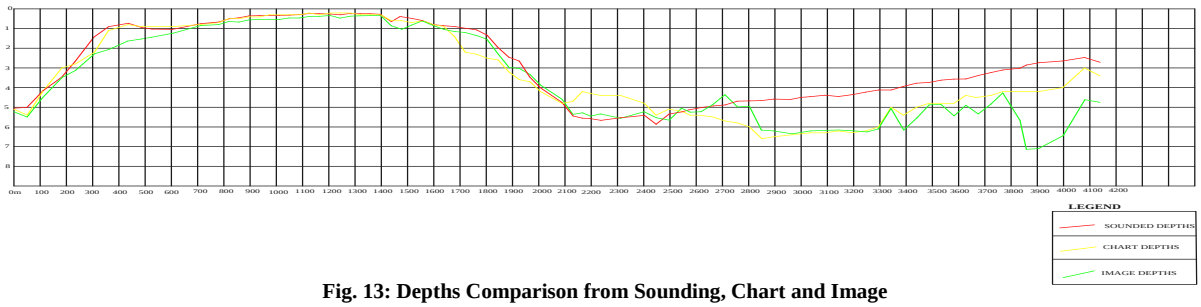

Fig. 13: Depths Comparison from Sounding, Chart and Image

From Figure 13, it was observed that the trend of the three sets of depths (sounding, chart and image depths depicted with red, yellow and green colours respectively) values showed similar patterns, but some variations towards the end. That is, 3.35km to 4.20km, the chart (yellow) and sounded depths plots (red) followed similar patterns but with difference (1m) in depths, but, notable disparity in image depths plots (green). These differences could have been attributed to various reasons, such as, certain changes on the seabed over the years due to human activities, outliers from noise, or attributed to possible variable bottom types (muddy and sandy) within the area which were not classified.

.

In the second instance, randomly selected points were spread horizontally across the image area in three sections (lower, middle and upper) where depths information on the Admiralty Chart were extracted, to examine the relationship between the derived image depths and chart depths. The derived image depths were extracted from the corresponding depth positions on the two generated images (from blue/green and blue/red ratios). Tables III, IV and V show values from the chart depths and image depths with their corresponding errors for the lower (section A), middle (section B), and upper (section C) respectively, while, Figures 14, 15 and 16 show the profile of the seabed for the different sections respectively

Table III: Compared Chart Depth with Derived Image Depths for Section A

S/N	LATITUDES	LONGITUDES	NORTHINGS	EASTINGS	CHART EPTHS	IMAGE DEPTHS (BLUE/RED)	IMAGE DEPTHS (BLUE/GREE N)	DIFF (B/R)	DIFF (B/G)
SECTION A									
1.	4 28 12.00	8 14 42.00	494122.373	416238.832	8.60	8.10	7.00	0.50	1.60
2.	4 28 24.00	8 15 30.00	494489.354	417718.513	6.70	7.20	6.30	-0.50	0.40
3.	4 28 36. 00	8 16 42.00	494855.628	419937.820	6.00	6.80	6.40	-0.80	-0.40
4.	4 28 24.00	8 17 36.00	494485.525	421601.660	7.30	7.30	6.90	0.00	0.40
5.	4 28 36.00	8 19 30.00	494850.703	425115.297	6.30	6.70	6.60	-0.40	-0.30
6.	4 28 30.00	8 20 42.00	494664.452	427334.037	7.50	7.00	6.80	0.50	0.70
7.	4 28 30.00	8 21 30.00	494663.146	428813.304	7.00	6.60	6.70	0.40	0.30
8.	4 28 30.00	8 22 12.00	494662.026	430107.660	5.60	5.20	5.70	0.40	-0.10
9.	4 28 30.00	8 23 52.00	494659.389	433188.024	4.30	4.00	4.20	0.20	0.10
10.	4 28 36.00	8 25 48.00	494840.824	436764.446	6.10	5.80	6.20	0.30	-0.10
11.	4 28 30.00	8 26 42.00	494654.312	438428.453	5.00	5.60	5.90	-0.60	-0.90
12.	4 28 42.00	8 27 41.00	495022.407	440234.004	4.20	4.00	4.00	0.20	0.20

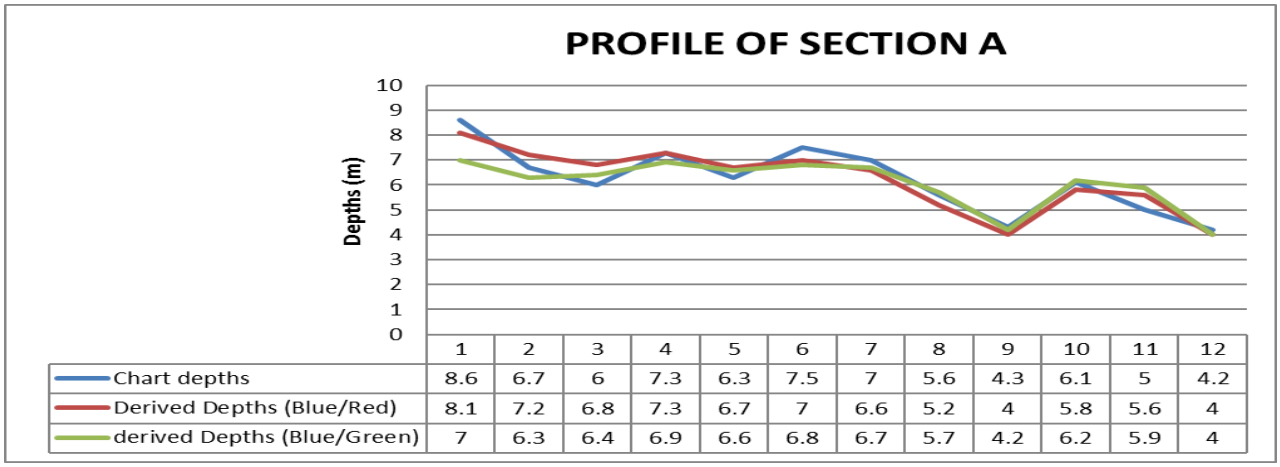

	1	2	3	4	5	6	7	8	9	10	11	12
Chart depths	8.6	6.7	6	7.3	6.3	7.5	7	5.6	4.3	6.1	5	4.2
Derived Depths (Blue/Red)	8.1	7.2	6.8	7.3	6.7	7	6.6	5.2	4	5.8	5.6	4
derived Depths (Blue/Green)	7	6.3	6.4	6.9	6.6	6.8	6.7	5.7	4.2	6.2	5.9	4

Fig. 14: Profile Plot of Chart Depths and Derived Image Depths for Section A

Table IV: Compared Chart Depth with Derived Image Depths for Section B

S/N	LATITUDES	LONGITUDES	NORTHINGS	EASTINGS	CHART DEPTHS	IMAGE DEPTHS (BLUE/ RED)	IMAGE DEPTHS (BLUE/ GREEN)	DIFF (B/R)	DIFF (B/G)
SECTION B									
1.	4 36 42.00	8 21 00.00	509771.651	427902.339	7.50	7.00	7.20	0.50	0.30
2.	4 36 48.00	8 21 48.00	509954.556	429381.492	6.20	6.50	6.00	-0.30	0.20
3.	4 36 48.00	8 22 24.00	509953.572	430490.727	5.00	5.20	5.30	-0.20	-0.30
4.	4 36 54.00	8 23 12.00	510134.423	431969.863	6.00	5.20	6.10	0.80	-0.10
5.	4 36 48.00	8 24 24.00	509955.147	434188.164	6.70	6.20	6.40	0.50	0.30
6.	4 36 42.00	8 25 12.00	509764.950	435666.982	4.10	4.90	5.30	-0.80	-1.20
7.	4 36 42.00	8 26 48.00	509762.597	438624.916	6.10	6.70	6.10	-0.60	0.00
8.	4 36 37.00	8 26 06.00	509596.829	437330.676	2.00	4.60	5.10	-2.60	-3.10
9.	4 36 36.00	8 26 24.00	509578.938	437885.289	3.60	5.90	5.70	-2.30	-2.10
10.	4 36 36.00	8 27 36.00	509577.226	440103.738	5.20	5.70	5.40	-0.50	-0.20
11.	4 36 36.00	8 27 54.00	509576.808	440658.349	5.00	6.40	5.90	-1.40	-0.90

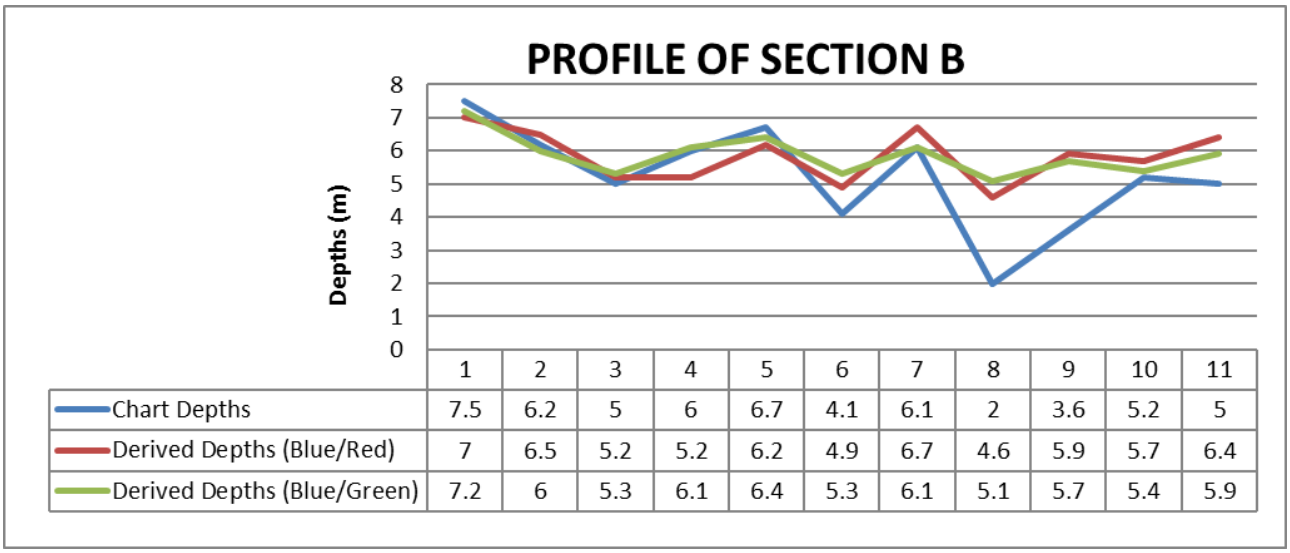

	1	2	3	4	5	6	7	8	9	10	11
Chart Depths	7.5	6.2	5	6	6.7	4.1	6.1	2	3.6	5.2	5
Derived Depths (Blue/Red)	7	6.5	5.2	5.2	6.2	4.9	6.7	4.6	5.9	5.7	6.4
Derived Depths (Blue/Green)	7.2	6	5.3	6.1	6.4	5.3	6.1	5.1	5.7	5.4	5.9

Fig. 15: Profile Plot of Chart Depths and Derived Image Depths for Section B

Table V: Compared Chart Depth with Derived Image Depths for Section C

S/N	LATITUDES	LONGITUDES	NORTHINGS	EASTINGS	CHART DEPTHS	IMAGE DEPTHS (BLUE/ RED)	IMAGE DEPTHS (BLUE/ GREEN)	DIFF (B/R)	DIFF (B/G)
SECTION C									
1.	4 41 18.00	8 19 54.00	518248.634	425872.740	5.20	6.20	5.70	1.00	-0.50
2.	4 41 36.00	8 20 30.00	518800.308	426986.385	6.20	6.30	6.30	-0.10	-0.10
3.	4 41 18.00	8 20 48.00	518247.066	427540.427	4.20	5.60	6.40	-1.40	-2.20
4.	4 41 18.00	8 22 30.00	518244.200	430668.933	5.40	5.20	5.50	0.20	-0.10
5.	4 41 18.00	8 23 12.00	518243.057	431976.901	3.20	3.00	3.50	0.20	-0.30
6.	4 41 12.00	8 23 54.00	518057.697	433270.708	2.30	2.60	2.60	-0.30	-0.30

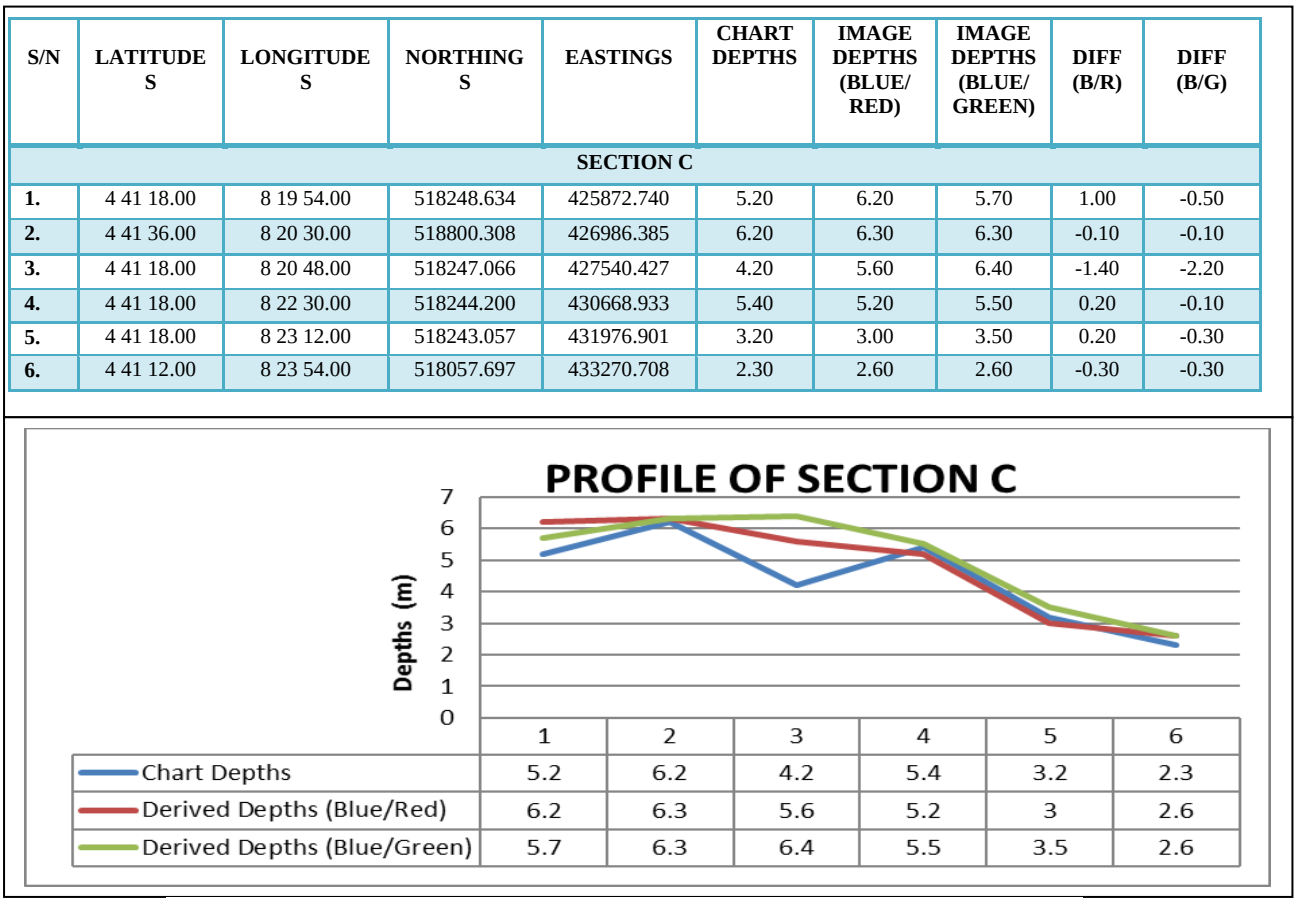

Fig. 16: Profile Plot of Chart Depths and Derived Image Depths for Section C

ii) Assessment of Image Depths

The derived image depths were evaluated against sounded data and corresponding chart depths. Thereafter sample data from the Admiralty Chart of Approaches to Calabar (Chart No. 3433) were used to assess the derived image depths of the entire study area. The accuracy of the derived image depths from the Ratio Model yielded a good result when compared with the chart depths.

The accuracy of the derived image depths was evaluated against: 1) the sounded depths data and 2) extracted chart depths data. For the portion where sounding investigation was performed, Coefficient of Determination, R^2 = 0.821, was achieved by regressing image depths (generated from the blue/red ratio) against sounded depths (Figure 17). And a standard error of 0.246m, root mean square (rms) error of 0.346 and percentage relative error of 11.44% were obtained.

Similarly, assessment of the accuracy of the sounded depths in relation with the chart depths revealed a Coefficient of Determination of, R^2 = 0.871 (see Figure 18).

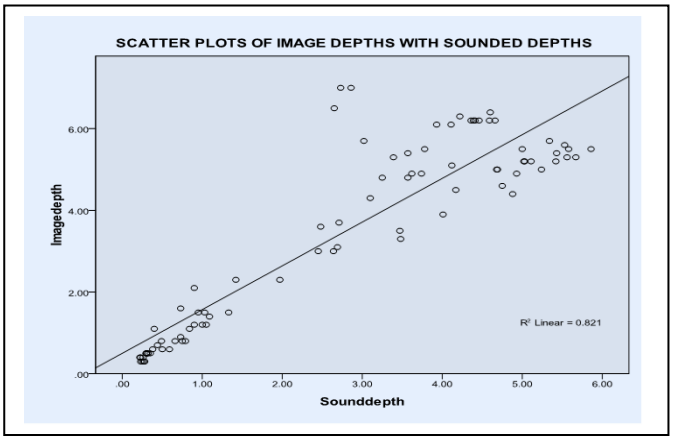

Fig. 17: Derived Image and Sounded Depths Correlation (Blue/red ratio).

In another assessment, all the extracted depths (29 number) values from the three Sections of the derived image and chart were also used in the evaluation. The Coefficients of Determination, R^2, of the image depths were 0.716 and 0.667 for blue/red and blue/green ratios respectively (Figures 19 and 20).

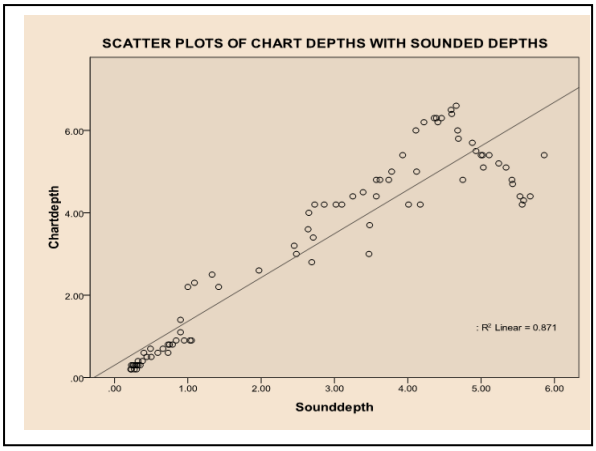

Fig. 18: Chart Depths and Sounded Depths Correlation.

In Figure 19 below, the accuracy of the derived image depths of blue/red ratio against chart depths showed a standard error of 0.236m, root mean square (rms) error of 0.556, and percentage relative error 11.672

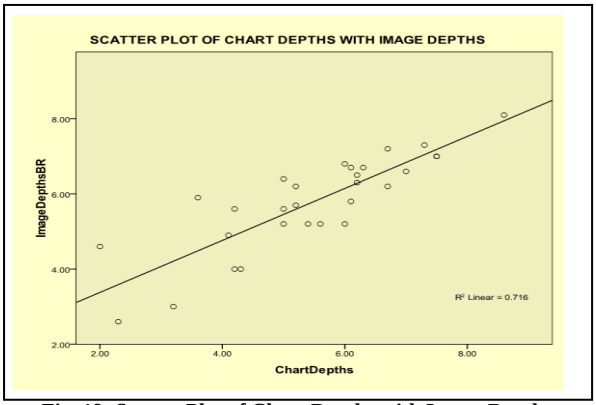

Fig. 19: Scatter Plot of Chart Depths with Image Depths generated from Blue/Red ratio

Whereas, for the derived image depths from blue/green ratio, revealed a standard error of 0.198m, root mean square (rms) error of 0.542, and relative percentage error of 11.167% were obtained (figure 20).

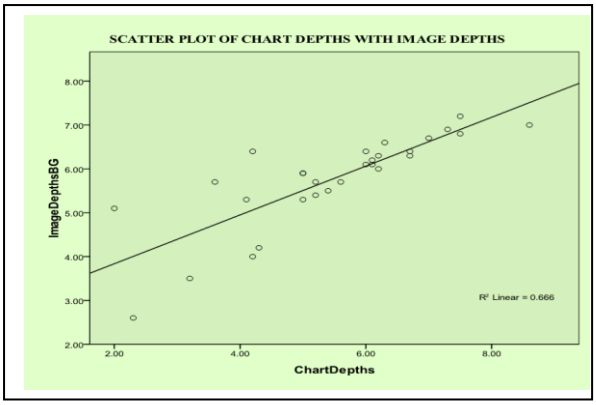

Fig. 20: Scatter Plot of Chart Depths with Image Depths generated from Blue/Green ratio

B. Discussions

The coefficient of Determinations R^2, which were 72% and 67% by regressing image depths against chart depths from the blue/red and blue/green algorithms respectively meant that the correlation analyses were good. That is, the 29 depths points randomly selected from cross sections showed good correlations. The criteria for the 29 points ensured that varying depths values along each cross sections were selected since large expand of seabed had almost the same height values. "Reference [1] used 25 training points to perform regression analyses of derived depths over the nautical chart depths for Kure Atoll in Northwestern Hawaiian Island covering 2,000km in length and 180km wide". And the results of the coefficient of determination revealed that the numbers of variations from blue/red ratio were more than those obtained from blue/green ratio, which also confirmed the fact that blue/red ratio captured more accurate depths information than blue/green ratio in the shallow areas.

From the results of analyses, the blue/green ratio yielded a standard error of 0.198m, root mean square (rms) error of 0.542, and relative percentage error of 11.167%, while the blue/red derived image depths revealed a standard error of 0.236m, root mean square (rms) error of 0.556, and percentage relative error 11.672%. Somehow the estimated image depths from blue/green ratio were slightly closer to their corresponding chart depths than those from blue/red ratio for areas where depths were greater than 5m. It is also believed that with increased number of sample points (from 29 to 50 points), the accuracy of the derived bathymetry would have improved. Again, "Reference [1] asserted that in an environment with multiple bottom types and depths variations, the standard error is amplified with limited data".

Considering also the extent to which ground-truth depths was obtained (4.2km sounding distance compared to a cross-sectional distance of 16km). The accuracy of the derived image depths when regressed against the ground-truth sounded depths showed a coefficient of determination, R^2, of 82%, a standard error of 0.246m and a root mean square (rms) error 0.346. These represented a good accuracy of the derived image depths for the extent where sounding investigation was performed. But due to the limitation in inadequate coverage of ground-truth depths, its usage for a thorough accuracy assessment of the study was hindered. These results further explained that reliable depths estimates could be derived from Ratio Model over unclassified variable bottom types of coastal waters when compared with results obtained in other studies. "Reference [11], validated the use of MeRIS image with 300m spatial resolution to map bathymetry of large areas of the Gulf of Lion in France, and obtained a relative percentage error of 16% and rms error of 9.36 for depth range of 20m – 50m". In another study by "Reference [16], three methodologies – Lyzenga, Jupp and Stumpf's Models

were employed on hyperspectral and multispectral imagery for bathymetry estimation. The extracted results showed that Stumpf's (Ratio) Model gave the best fit in terms of Coefficient of Determination, R^2 = 0.869, standard error = 0.99m and percentage relative error = 7.46% considering the complexities of the area, which was classified as a non-homogeneous environment".

The intervals of years between the three datasets used in this study was also an issue of concern. For the Admiralty Chart itself (edited in 1994), the data were acquired from three different sources and years – Nigerian Port Authority (NPA) Surveys (in 1990), Commercial surveys (in 1979) and Admiralty surveys (in 1911). Whereas, Lansat-7 ETM+ imagery was acquired in 2000, while sounding was performed in 2011. This revealed the duration of years between the chart, image and sounding. Apparently, certain morphological changes could have occurred on the seabed within these years as a result of human activities, tidal influences, etc. Hence, the possible reason for notable variations on the seabed topography in the three datasets.

In the same vein, observing the derived depths values in Tables III – V, when compared with chart depths, revealed that some were either over-estimated or under-estimated. This could have been caused by possible variable seabed within the study area, which were not classified. Studies have revealed that sandy seabed produces higher reflectance values than other bottom types especially in very shallow water areas, resulting in overestimate of the depth values. This could also be attributed to the high values of apparent reflectance in the green band. The green band being one of the denominators in the ratio model, therefore produced results close to zero as the reflectance increases. In view of this, it could substantiate why greater depths values were seen in the image depths in Section B. This also affirms "Reference [17], assertion that the ratio algorithm is robust even when ground truth data about variable bottom types were unavailable, and that the blue/green ratio algorithm mostly was not suitable for depths estimation in shallow areas where depths were less than 5m".

IV. CONCLUSION

The use of Stumpf's Ratio model on medium resolution Landsat-7 ETM+ imagery to derived water depths of unclassified seabed morphology yielded good results comparatively. That is, in spite of the possible effects of depths generalization by 30x30m pixel values of Landsat-7 ETM, and variable bottom types, the accuracy of the derived bathymetric depths were good indicators of the actual bathymetry of Cross River. Therefore, the model demonstrated its strength to estimate bathymetric depths of coastal shallow waters with limited ground-truth depths, over unclassified variable bottom types.

The ratio of blue/red wavelength employed in the model produced a better representation of the depths in shallow water regions when compared to those of blue/green wavelength. And the accuracies implied that Landsat-7 ETM+ derived depths were dependable as an aid to rapid monitoring of coastal shallow waters seabed topography. Thus, it is imperative to note that the derivation of bathymetric depths using remote sensing technique is a reliable alternative approach to the conventional ship-based sonar method in terms of economic reasons, efficiency and safety.

It is also essential to observe that the use of high resolution multispectral images, such as, IKONOS, QuickBird, etc., would further improve the accuracies of the derived bathymetric depths.

REFERENCES

[1] Camacho, M. A., "Depth analysis of midway atoll using Quickbird multi-spectral imaging over variable substrates". M.Sc. Thesis, Dept. of Space System, Naval Postgraduate School, Monterey, California, 2006.

[2] Chander, G., Markham, B. L., and Helder, D. L., "Summary of current radiometric coefficients for Landsat MSS, TM, ETM, and EO-1 ALI sensors". Remote Sensing of Environment 113: 893-903, 2009.

[3] Chavez, P. S. Jr., "Image-based atmospheric correction – revisited and improved". Photogrammetric Engineering & Remote Sensing, 62(9): 1025 – 1036, 1996.

[4] Fisher, T. M., "Shallow water bathymetry at lake tahoe from AVIRIS data". M.Sc. Thesis, Dept. of Oceanography, Naval Postgraduate School, Monterey, California, 1999.

[5] Gordon, H. R., Clark, D. K., Brown, W. J., Brown, O. B., Evans, R. H., Broenkow, W. W., "Phytoplankton pigment concentration in the Middle Atlantic Bight: comparison of ship determinations and CZCS Estimates". Applied Optics 22: 20-36, 1983.

[6] Green, E. P., Mumby, P. J., Edwards, A. J., Clark, C. D., Remote sensing handbook for tropical coastal management. Coastal Management Sourcebooks 3, UNESCO, Paris, 2000.

[7] Haibin Su, Hongxing Liu, Heyman, W. D., "Automated derivation of bathymetric information from multi-spectral satellite imagery using a non-linear Inversion model". *Marine Geodesy, 31: 281-298*, 2008.

[8] Huang, C., Yang, L., Homer, C., Wylie, B., Vogelman, J., and DeFelice, T., "At-satellite reflectance: a first order normalization of Landsat-7 ETM+ images". United States Geological Survey, Raytheon ITSS, EROS Data Centre, Sioux Falls, USA, 2002.

[9] Loomis, M. J., "Depth derivation from the Worldview-2 satellite using hyperspectral imagery". *M.Sc. Thesis in Dept. of Meteorology, Naval Postgraduate School, Monterey, California*, 2009.

[10] Melsheimer, Christian and Chin, Liew Soo, "Extracting bathymetry from multi-temporal SPOT images". Paper presented at the 22nd Asian Conference on Remote Sensing 5-9 November 2001, Singapore, 2001.

[11] Minghelli-Roman, A., Polidori, L., Mathieu-Blanc, S., Loubersac, L. and Cauneau, F., "Bathymetry estimation using MeRIS images in coastal sea waters". IEEE Geoscience and Remote Sensing Letters, 4(2), 2007.

[12] Mishra, D., Narumalani, S., Lawson, M., and Rundquist, D., "Bathymetric mapping using multispectral data". GIScience and Remote Sensing, 41(4): 301 – 321, 2004.

[13] Nurlidiasari, Marlina, "The application of Quickbird and multitemporal Landsat TM data for coral reef habitat mapping. Case study: derawan Island, east kalimantan, Indonesia". International Institute for Geo-Information Science and Earth Observation. Enchede, The Netherlands, 2004.

[14] Ojinnaka, O. C., "Charting the waters of the developing nations with focus on Nigeria". *The Hydrographic Journal, London 8,* 1997.
[15] Ojinnaka, O. C., "University of Nigeria tidal analysis and prediction program (UNITAPP), A Monograph on Tidal Analysis and Prediction". Department of Geoinformatics and Surveying, University of Nigeria, Enugu Campus, Nigeria, 2008.
[16] Pennucci, G., Grasso, R., and Trees, C., "A study of near-shore characterization using high-resolution hyperspectral and multispectral images". NURC, NATO Research Centre, Military and Oceanographic Department, La Spezia, Italy, 2008.
[17] Stumpf, R. P., Holderied, K., and Sinclair, M., "Determination of water depth with high-resolution satellite imagery over variable bottom types". Limnology and Oceanography, 48(1, part 2): 547-556, 2003.
[18] Zhongwei D. and Minhe Ji, Z. Z., "Mapping bathymetry from multi-source remote sensing images: A case study in the beilun estuary, guangxi, china". The International Archives of the Photogrammetry, Remote Sensing and Spatial Information Sciences. XXXVII: Part B, (2008).
[19] Available Website [Online] http://earth.gis.usu.edu/imagestd.